Arteriosclerosis, Thrombosis, and Vascular Biology

BASIC SCIENCES

Mitochondrial Ca^{2+} Uptake Drives Endothelial Injury By Radiation Therapy

Karima Ait-Aissa, Olha M. Koval, Nathanial R. Lindsey, Isabella M. Grumbach

BACKGROUND: Radiation therapy strongly increases the risk of atherosclerotic vascular disease, such as carotid stenosis. Radiation induces DNA damage, in particular in mitochondria, but the upstream and downstream signaling events are poorly understood. The objective of this study was to define such mechanisms.

METHODS: Endothelial-specific MCU (mitochondrial Ca^{2+} uniporter) knockout and C57Bl6/J mice with or without a preinfusion of a mitoTEMPO (mitochondrial reactive oxygen species [ROS] scavenger) were exposed to a single dose of cranial irradiation. 24, and 240 hours postirradiation, vascular reactivity, endothelial function, and mitochondrial integrity were assessed ex vivo and in vitro.

RESULTS: In cultured human endothelial cells, irradiation with 4 Gy increased cytosolic Ca^{2+} transients and the mitochondrial Ca^{2+} concentration ($[Ca^{2+}]_{mt}$) and activated MCU. These outcomes correlated with increases in mitochondrial ROS ($_{mt}$ROS), loss of NO production, and sustained damage to mitochondrial but not nuclear DNA. Moreover, irradiation impaired activity of the ETC (electron transport chain) and the transcription of ETC subunits encoded by mitochondrial DNA ($_{mt}$DNA). Knockdown or pharmacological inhibition of MCU blocked irradiation-induced $_{mt}$ROS production, $_{mt}$DNA damage, loss of NO production, and impairment of ETC activity. Similarly, the pretreatment with mitoTEMPO, a scavenger of $_{mt}$ROS, reduced irradiation-induced Ca^{2+} entry, and preserved both the integrity of the $_{mt}$DNA and the production of NO, suggesting a feed-forward loop involving $[Ca^{2+}]_m$ and $_{mt}$ROS. Enhancement of DNA repair in mitochondria, but not in the nucleus, was sufficient to block prolonged $_{mt}$ROS elevations and maintain NO production. Consistent with the findings from cultured cells, in C57BL/6J mice, head and neck irradiation decreased endothelium-dependent vasodilation, and $_{mt}$DNA integrity in the carotid artery after irradiation. These effects were prevented by endothelial knockout of MCU or infusion with mitoTEMPO.

CONCLUSIONS: Irradiation-induced damage to $_{mt}$DNA is driven by MCU-dependent Ca^{2+} influx and the generation of $_{mt}$ROS. Such damage leads to reduced transcription of mitochondrial genes and activity of the ETC, promoting sustained $_{mt}$ROS production that induces endothelial dysfunction. Our findings suggest that targeting MCU and $_{mt}$ROS might be sufficient to mitigate irradiation-induced vascular disease.

GRAPHIC ABSTRACT: A graphic abstract is available for this article.

Key Words: calcium ■ carotid stenosis ■ endothelium ■ mitochondria ■ reactive oxygen species

Of the 1.8 million Americans who are diagnosed with a malignancy every year, ≈50% will undergo radiation therapy as part of their cancer treatment. In light of novel therapies with increased efficacy for many cancers, the number of survivors is expected to increase to ≈25 million by 2030.[1] However, radiation therapy strongly increases the risk of atherosclerotic vascular disease in proximity to the radiation field in cancer survivors.[2,3] As such, radiation therapy for breast, lung, and esophageal cancer as well as for lymphoma promotes coronary disease. Moreover, radiation therapy for head and neck cancer increases the risk of carotid artery stenosis because of the proximity of the carotid artery to the lymphatic structures that are targeted by this treatment.[4-6]

See accompanying editorial on page 1137

Correspondence to: Isabella Grumbach, MD, PhD, University of Iowa, Carver College of Medicine, Division of Cardiovascular Medicine, 4338 PBDB, 169 Newton Rd, Iowa City, IA, 52242, Email isabella-grumbach@uiowa.edu; or Karima Ait-Aissa, PhD, University of Iowa, Carver College of Medicine, Division of Cardiovascular Medicine, 4330 PBDB, 169 Newton Rd, Iowa City, IA, 52242, Email karima-ait-aissa@uiowa.edu
Supplemental Material is available at https://www.ahajournals.org/doi/suppl/10.1161/ATVBAHA.122.317869.
For Sources of Funding and Disclosures, see page 1134.

Arterioscler Thromb Vasc Biol is available at www.ahajournals.org/journal/atvb

Nonstandard Abbreviations and Acronyms

$\Delta\psi_{mt}$	mitochondrial membrane potential
AUC	area under the curve
ECs	endothelial cells
ETC	electron transport chain
HCAECs	human coronary artery endothelial cells
HUVECs	human umbilical endothelial cells
MCU	mitochondrial Ca^{2+} uniporter
mitoTEMPO	mitochondrial reactive oxygen species scavenger
$_{mt}$DNA	mitochondrial DNA
$_{mt}$ROS	mitochondrial reactive oxygen species
MTT	mitochondrial TEMPO
$_{nuc}$DNA	nuclear DNA
OGG1	8-oxoguanine glycosylase 1α
PCR	polymerase chain reaction

Highlights

- In human endothelial cells, irradiation induced a feed-forward circuit of mitochondrial Ca^{2+} entry and superoxide production driven by a hyperpolarized membrane potential that induced mitochondrial DNA damage and loss of nitric oxide.
- Transcription of ETC (electron transport chain) subunits from mitochondrial, but not nuclear, DNA and activity of the ETC (electron transport chain) were reduced after irradiation but preserved by concomitant mitochondrial superoxide scavenging or MCU (mitochondrial Ca^{2+} uniporter) blockade.
- Enhancement of DNA repair in mitochondria normalized mitochondrial reactive oxygen species and NO production following irradiation.
- Endothelial MCU knockout or infusion with the mitochondrial superoxide scavenger mitoTEMPO (mitochondrial reactive oxygen species scavenger) decreased endothelium-dependent vasodilation and mitochondrial DNA integrity in the carotid artery at 24 and 240 hours after irradiation.

The high prevalence of atherosclerotic vascular disease in adult cancer survivors is due in part to their shared risk factors, including tobacco use and older age. However, data from childhood cancer survivors demonstrate that irradiation is an independent multiplicative risk factor for the development of atherosclerotic disease,[7] implying that irradiation induces molecular events additional to those provoked by established risk factors for atherosclerosis. Yet, these events have been incompletely elucidated.

One major cause of irradiation-induced vascular disease is believed to be acute injury to endothelial cells, which are known to be highly sensitive to irradiation.[8] The injury initiates long-term signaling events that ultimately promote atherosclerosis. Indeed, one study showed that at 4 to 6 weeks after radiation therapy, human carotid arteries exhibited significant impairment of endothelium-dependent dilation in response to NO and prostacyclin, whereas constriction, which is mediated by smooth muscle cells, was unaffected.[9] These findings also support the notion that endothelial dysfunction is a clinically relevant indicator of carotid injury after radiation therapy.

Exposure to radiation leads to an acute burst of reactive oxygen species (ROS) and free radicals[10]; this is followed by chronic production of ROS, which in turn fuels inflammation. Currently, the events that promote progression from acute to chronic elevations in ROS are not well understood.[11,12] One potential mechanism is mitochondrial injury[13] as the excess free radicals could conceivably reduce the activity of the ETC (electron transport chain) as well damage the mitochondrial DNA ($_{mt}$DNA) in endothelial cells. These events could ultimately lead to a chronic elevation in ROS production.[14,15]

Altered cytosolic Ca^{2+} transients and decreased endoplasmic reticulum Ca^{2+} load after irradiation have been reported in the past.[16] Yet, our understanding of how irradiation affects mitochondrial Ca^{2+} handling and endothelial cell function is spurious. We previously observed that blocking mitochondrial Ca^{2+} entry by inhibiting the MCU (mitochondrial Ca^{2+} uniporter) is sufficient to protect against both the production of excess ROS after irradiation.[17] Irradiation induces the oxidation of Fe/sulfur clusters of ETC subunit I and thereby, impairs ETC activity and induces high steady-state levels of $O_2^{\bullet-}$ and H_2O_2.[18,19] Mitochondrial Ca^{2+} entry enhances metabolic activity by activating trichloroacetic acid (TCA) cycle dehydrogenases upstream of the ETC[20] and may accelerate ETC dysfunction after irradiation.

Here, we sought to determine whether reducing Ca^{2+} entry or reducing mitochondrial ROS ($_{mt}$ROS) production during radiation therapy is sufficient to prevent short- and long-term endothelial dysfunction and to establish the underlying mechanisms, in addition to testing how acute injury induces sustained endothelial dysfunction. Specifically, we investigated whether in vivo scavenging of mitochondrial superoxide or selective endothelial deletion of MCU is sufficient to protect endothelial function during head and neck irradiation and how these interventions affect mitochondrial Ca^{2+} handling, membrane potential ($\Delta\psi_{mito}$), $_{mt}$ROS levels, DNA integrity, and NO bioavailability. We also provide proof-of-concept data supporting that such novel mitigators would be effective.

MATERIALS AND METHODS

All raw data, analytical methods, and study materials that support the findings of this study are available from the corresponding authors upon reasonable request.

Reagents

Phenylephrine (no. 0754) was obtained from Amresco, acetylcholine (no. A6625), and sodium nitroprusside (S0501) were obtained from Sigma-Aldrich, and N(gamma)-nitro-L-arginine methyl ester (L-NAME, no. 483125) was obtained from EMD Millipore.

Human coronary artery endothelial cells (HCAECs) were kindly provided by Dr Gerene Denning (University of Iowa), and human umbilical endothelial cells (HUVECs, no. PCS-100-013) were obtained from American Type Culture Collection. Endothelial cells (ECs) were grown in endothelial cell medium supplemented with growth factors (no. 1001, ScienCell).

Transfection was performed using Opti-MEM I medium (Gibco, 31985–062) and Lipofectamine 2000 (Thermofisher). MitoTEMPO (mitochondrial reactive oxygen species [ROS] scavenger; no. SML0737) was obtained from Enzo. MitoSOX Red (no. D1168) and MitoTracker Green FM (no. M7514) were obtained from ThermoFisher. Tetramethylrhodamine methyl ester (no. T668) was purchased from Molecular Probes.

The following antibodies were obtained from Cell Signaling Technology and used for immunoblotting: anti-MCU (no. 14997), anti-GAPDH (no. 2178), and anti-c-Myc (cellular myelocytomatosis; no. 5605). Phosphorylated (Ser92) MCU was kindly provided by Dr Anderson Lab (Johns Hopkins University).

siRNAs and Plasmids

Scrambled and silencer (si)RNAs against MCU were obtained from Integrated DNA Technologies.

Plasmids encoding mitochondria-targeted (mito-; no. 18706), mutant mitochondria-targeted (mutt; no. 18708), and nucleus-targeted (nuc-) OGG1-α (8-oxoguanine-DNA glycosylase 1-α; no. 18709) were generated and deposited by Dr Sidransky[21] (Addgene). The small-molecule MCU inhibitor RU265 was kindly provided by Dr Woods, Cornell University.[22]

Mice

All experimental procedures were approved by the Institutional Animal Care and Use Committees of both the University of Iowa and the Iowa City VA Health Care System and complied with the standards of the Institute of Laboratory Animal Resource, National Academy of Science. The C57BL/6J male and female mice used in the described experiments were obtained from The Jackson Laboratory (no. 000664). Specific MCU deletions were studied in mice in which exons 5 and 6 of MCU are flanked by loxP sites.[23] These mice were purchased from Jackson Laboratory (no. 029817). Endothelial MCU knockout mice ($eMCU^{-/-}$) were generated by mating $MCU^{fl/fl}$ mice with counterparts carrying a transgene encoding tamoxifen-inducible Cre recombinase, with expression controlled by the Tie2 promoter.[24] Cre recombination was induced by intraperitoneal injection of tamoxifen (80 mg/Kg) for 5 days, followed by a 14-day break, and then an identical second course of tamoxifen treatment.[25] Littermate $MCU^{fl/fl}$ mice that lacked the *cre* allele but were treated with tamoxifen served as controls for all experiments. All mice used were from 12 to 16 weeks of age at the time of treatment; male and female mice were used in equal proportions. Data from male and female mice were analyzed separately initially. The results reported in this article were combined because no difference was seen between the 2 groups regardless of sex. Correct recombination and MCU were confirmed by quantitative reverse-transcription polymerase chain reaction (PCR) and imaging of mitochondrial Ca^{2+} transients with $_{mt}$Pericam (mitochondria-targeted genetic Ca^{2+} indicator Pericam).

Radiation Exposure in Mice

When mice were at least 12 weeks of age, they were anesthetized with ketamine and xylazine and received a single dose (12 Gy) of X-rays (irradiation) to the whole brain. This treatment was administered using an XStrahl Small Animal Radiation Research Platform,[26] which incorporates a 60 kVp beam of 0.2 mm Al quality for use in Cone Beam CT acquisition and a 220 kVp 0.63 mm Cu quality beam for use in treatment-type irradiation. The dose of 12 Gy was chosen because it is the equivalent of 2 Gy fractions of 40 Gy,[27] which is within the range used in humans for radiation therapy in head and neck cancer. Control animals were sham irradiated (anesthetized and placed in the radiation chamber only).

Mitochondrial ROS Scavenging In Vivo

For scavenging mitochondrial superoxide in mice, mitochondrial TEMPO (MTT)[28] was administered for 14 days by continuous infusion, using osmotic mini-pumps, at a dose of 0.7 mg/kg per day. The mini-pumps were implanted 3 days before irradiation. Control animals were implanted with osmotic mini-pumps filled with normal saline.

Measurement of Vascular Reactivity

The carotid and second-branch mesenteric resistance arteries were carefully cleaned of fat and connective tissue and then cut into rings 2 mm in length. These arterial rings were mounted in a small vessel dual-chamber myograph and isometric tension was measured. The arteries were then equilibrated in Krebs solution bubbled with carbogen at 37 °C and pH 7.4 for 30 minutes and stretched to their optimal physiological lumen diameter for active tension development for 1 hour. The vascular rings were then preconstricted with phenylephrine (3.10^{-5} M). Once a steady maximal contraction was reached, cumulative concentration-response curves were obtained for acetylcholine (10^{-8}–3×10^{-5} M) and sodium nitroprusside (10^{-8}–3×10^{-5} M).

Endothelial Cell Cultures and Treatments

Primary HCAECs and HUVECs were grown in endothelial cell medium at 37 °C and 5% CO_2 and used at passages 3 to 5.

siRNA Transfection

ECs were transfected with 5 nmol/L of siRNA duplexes targeting MCU (siMCU; 5′–CGACCUAGAGAAAUACAAUCAGCTC–3′ and 5′–GGGAAUAAAGGGAUCUUAAAUGCTG–3 at a 1:1 ratio) or scrambled control (5′–CGUUAAUCGCGUAUAAUACG CGUA–3′, Integrated DNA Technologies) in Lipofectamine RNAiMaX reagent following the manufacturer's instructions. Transfection was performed 48 hours before irradiation. After 48 hours, knockdown efficiency was assessed by Western blotting for MCU. The efficiency of knockdown was consistently >75%.

MTT Treatment

ECs were treated with 10 μM MTT in dimethyl sulfoxide (DMSO) for 18 hours before irradiation. Control cells were treated with DMSO only.

Irradiation

Once ECs were 80% confluent, they were exposed to 4 Gy. Ionizing radiation was delivered at 1.29 Gy/min using a cesium-137 γ-ray source in the Radiation and Free Radical Research Core of the University of Iowa. At 24, 48, 120, and 240 hours following irradiation, ECs were collected for analyses of mRNA levels, protein levels, or imaging.

Cytosolic Ca^{2+} Measurement

HCAECs were cultured on 35-mm glass-bottom microwell dishes for 24 hours and after that used for analysis. Cells were incubated with the ratiometric indicator dye Fura-2 AM (1 μM, Invitrogen) in endothelial cell medium (endothelial cells phenol-free media) for 10 minutes at 37 °C. For recording of cytosolic Ca^{2+} transients, images were acquired continuously for at least 10 minutes every 5 seconds. After short baseline recording (15–20 s), thapsigargin (1 μM) was applied by micropipette injection. The cells were excited alternately at 340 and 380 nm. Fluorescence signal intensity was acquired at 510 nm. Data are presented as peak amplitude or area under the curve (AUC). Imaging was done with Nikon Eclipse Ti2 microscope under ×40 objective. Analysis was performed with NS Elements software (Nikon).

Measurement of Calcium Uptake by Mitochondria

Ratiometric measurements of $[Ca^{2+}]$ in mitochondria were performed in ECs that had been transduced with adenovirus expressing $_{mt}$Pericam for 48 hours.[29] Pericam fluorescence was quantified in ECs in Tyrode's solution at room temperature, using a customized Nikon Eclipse Ti2 inverted light microscope. Pericam was excited at 405 nm and 480 nm, and its emission was recorded at 535 nm. Recordings were performed every 5 s for at least 10 minutes. Real-time Pericam fluorescence ratios were recorded after PDGF (platelet-derived growth factor) was added (20 ng/mL) and were quantified using ImageJ. Peak amplitude (R) was calculated by subtracting the baseline fluorescence ratio from the peak fluorescence ratio. The AUC was determined by subtracting the AUC value obtained in the absence of agonist over the same recoding period. Summary data represent the average difference in basal and peak mitochondrial $[Ca^{2+}]$ ($[Ca^{2+}]_{mt}$).

Measurement of Mitochondrial ROS Production

Mitochondrial ROS production was measured in live-cultured HCAECs using the dihydroethidium derivative mitoSOX red (5 μM).[30] Cells were loaded with mitoSOX (final concentration 5 μM) and MitoTracker Green FM (final concentration 1 μM)[31] for 20 minutes at 37 °C. The cells were then rinsed, imaged using a NIKON microscope, and analyzed using National Institutes of Health ImageJ. All images were taken using the same settings. Specifically, mitoSOX and the MitoTracker Green FM signals were traced per cell and the fluorescence intensity of mitoSOX was normalized to that of MitoTracker Green FM. Data are presented as the ratio of integrated density mitoSOX signal to MitoTracker Green FM signal.

Quantification of NO Quantification

NO levels were measured using the fluorescent probe diaminofluorescein diacetate (Sigma).[32] Glass-bottom 35-mm dishes were seeded with HCAECs. At confluency, the HCAECs were briefly washed with Dulbecco's phosphate-buffered saline and then exposed to diaminofluorescein diacetate (final concentration 5 μmol/L, premixed with fresh endothelial cell medium) for 10 minutes. The HCAECs were then rinsed and imaged under a fluorescence microscope. To stimulate NO production, the HCAECs were treated with PDGF (20 ng/mL)+glutamine (1 μmol/L). Continuous imaging was performed for a period of 10 minutes following stimulation. The amount of NO produced is expressed as fluorescence intensity normalized to that at baseline.

Assessment of Damage to $_{mt}$DNA

Quantitative PCR was used to assay $_{mt}$DNA damage as described previously.[33] Briefly, total DNA was isolated using Genomic-tips and the Genomic DNA Buffer Set Kit (Qiagen, Valencia, CA). The purified DNA was quantified fluorometrically using Pico Green dsDNA reagent (Molecular Probes, Life Technologies). The Platinum PCR Super Mix (Invitrogen) was used to amplify 20 ng genomic DNA. Specific primers were used to amplify a long fragment of the $_{mt}$DNA (8.9 kb) to determine its integrity, as well as a short fragment (139 bp) to monitor changes in $_{mt}$DNA copy number and to normalize the data obtained from amplification of the 8.9-kb fragment. Ratios of relative amplification were calculated to compare $_{mt}$DNA damage in irradiated ECs to that in nonirradiated ECs; these values were used to express the number of lesions present in DNA, assuming a Poisson distribution, as previously described.[33]

Assessment of Damage to Nuclear DNA ($_{nuc}$DNA)

Total genomic DNA was purified from ECs using the DNeasy Blood & Tissue Kit (Qiagen). Quantity and purity of the DNA were determined by spectrometry using a Nanodrop 1000 instrument. SYBR Green PCR Master Mix complemented with Platinum Taq DNA Polymerase, High Fidelity (amplification capacity of 20 kb; Invitrogen) was used to amplify fragments from 20 ng of genomic DNA. Primers that amplify a long fragment of the nuclear gene β-globin (12 kb) were used to assess the integrity of the genomic DNA. Primers that amplify a short fragment of the nuclear gene *ESR1* (139 bp) were used for normalization to β-globin levels across samples.[34] Data were analyzed using the comparative Ct method. β-globin levels were normalized to those of the short fragment amplified from the *ESR1* gene and expressed as relative fold change.

Real-Time PCR

Total mRNA was harvested from HCAECs using a Qiagen RNeasy Kit. Approximately 1000 ng of RNA was used to synthesize cDNA using SuperScript VILO MasterMix (Invitrogen). Gene expression for ETC subunits was quantified by real-time-quantitative PCR using primers sets: mt-COI (cytochrome c oxidase I): Forward 5′-TCGCAATTCCTACCGGTGTC-3′ and reverse: 5′-CGTGTAGGGTTGCAAGTCAGC-3′; mt-ND1 (NADH-ubiquinone oxidoreductase chain 1): Forward 5′-GCACCTA CCCTATCACTCACA-3′ and reverse: 5′-GTTTGGGCTACG GCTCG-3′; NDUF1 (NADH dehydrogenase [ubiquinone] 1 alpha subcomplex subunit 1): Forward 5′-ATGTGGTTCGAG ATTCTCC-3′ and reverse: 5′-GCAACCCTTTTTTCCTTGC-3′;

COX11 (cytochrome c oxidase 11): Forward: 5′-AGGAAGAG AGTGGTGTTTTTTATTGGGTAAGTTGT-3′ and reverse: 5′-CA GTAATACGACTCACTATAGGGAGAAGGCTACCTTAACTA CCAAACTCCTC-3′, and ribosomal 18S forward 5′-CCCTAT CAACTTTCGATGGTAGTCG -3′, reverse 5′-CCAATGGATCCTC GTTAAAGGATTT -3′. Ribosomal 18S was used as internal gene control.

ETC Complex 1 Activity Assay

Complex 1 activity was measured in HCAECs lysates. The experiment was performed using the MitoCheck Complex I Activity Assay Kit (no. 700930, Cayman Chemical, Ann Arbor, MI) according to the manufacturer's instructions.

Targeting Mitochondrial DNA Repair

HCAECs and HUVECs were transiently transfected with plasmids encoding mito-, mutt-, and nuc- OGG1. Lipofectamine 2000 (Invitrogen) was used according to the manufacturer's instructions. Exogenous expression of mito-OGG1, mutt-OGG1, and nuc-OGG1 after transfection was verified by Western blotting using c-Myc antibody (Santa Cruz Biotechnology). At 48 hours post-transfection, the ECs were subjected to irradiation and, at 24 hours and 240 hours postirradiation, they were tested for $_{mt}$DNA damage as well as $_{mt}$ROS.

Statistical Analysis

Data are expressed as mean±SEM and were analyzed using the GraphPad Prism 9.0 software. For continuous variables, normality and homogeneity of variance were assessed by Shapiro-Wilk and Brown-Forsythe tests, respectively. Kruskal-Wallis test and Dunn post hoc test were used for data sets where normal distribution could not be assumed. Two-tailed unpaired Student *t* test and 1-way ANOVA, followed by Tukey multiple comparison test, were used for data sets with normal distribution. Two-way ANOVA followed by Tukey multiple comparison test was used for grouped data sets. A $P<0.05$ was considered significant.

RESULTS

Mitochondrial Ca^{2+} Entry Is Necessary for Irradiation-Induced $_{mt}$ROS Production and Endothelial Dysfunction

Previous studies had reported that irradiation leads to altered cytosolic Ca^{2+} handling and endoplasmic reticulum Ca^{2+} loading.[16] In this study, we first confirmed that endoplasmic reticulum Ca^{2+} loading is increased after irradiation in HUVECs 24 hours after irradiation. Knockdown of MCU before irradiation led to a decreased cytosolic Ca^{2+} transients assessed as thapsigargin-induced peak amplitude (Figure 1B) and AUC (Figure 1C; Figure 1A through 1C). The acute inhibition of the mitochondrial Ca^{2+} uniporter following irradiation, using the cell-permeable, selective small-molecule inhibitor Ru265, had the same effect (Figure S1A through S1C). At 24 hours after irradiation, the MCU was phosphorylated at Ser 92, indicating that the Ca^{2+} conducting activity of MCU was increased[35,36] (Figure 1D).

To directly test whether irradiation affects mitochondrial Ca^{2+} entry via MCU, mitochondrial Ca^{2+} levels were measured using the $_{mt}$Pericam. In control HUVECs, irradiation led to increases in both the baseline mitochondrial Ca^{2+} concentration ($[Ca^{2+}]_{mt}$ and PDGF-induced mitochondrial Ca^{2+} transients (assessed as AUC), at 24 postirradiation (Figure 1E through 1G). The converse was found in cells where MCU had been knocked down using a siRNA-mediated approach. Specifically, in such cells, irradiation led to reductions in the baseline $[Ca^{2+}]_{mt}$ and peak amplitude of PDGF-induced mitochondrial Ca^{2+} transients (AUC; Figure 1E through 1G).

Mitochondrial Ca^{2+} entry via the MCU complex is driven by the membrane potential ($\Delta\psi_{mt}$). Thus, we investigated the relationship between mitochondrial Ca^{2+} entry and the $\Delta\psi_{mt}$. Recordings of HUVECs with tetramethylrhodamine methyl ester at 24 and 240 hours after irradiation confirmed that the mitochondrial membrane is hyperpolarized in control HUVECs but not in counterparts transfected with an MCU siRNA (Figure 1H).

To confirm that an increase in $[Ca^{2+}]_{mt}$ following irradiation drives $_{mt}$ROS production, we measured mitochondrial superoxide production in primary HCAECs following siRNA-mediated MCU knockdown at 24 and 240 hours after irradiation. In these cells, irradiation failed to induce $_{mt}$ROS production or an increase in $\Delta\psi_{mt}$ (Figure 1I and 1J). Sustained increases in superoxide are known to reduce levels of nitric oxide (NO) by scavenging and eNOS uncoupling.[37,38] As anticipated, NO levels were reduced in control cells following irradiation, but preserved in counterparts in which MCU had been knocked down (Figure 1K and 1L).

Scavenging $_{mt}$ROS Protects From Irradiation-Induced Ca^{2+} Alterations, $_{mt}$DNA Damage, and Loss of NO Production in Endothelial Cells

Next, we tested the ability of the mitochondrial superoxide scavenger MTT to reduce $_{mt}$ROS and preserve NO production in HCAECs following irradiation. In irradiated HCAECs, levels of $_{mt}$ROS were 15-fold and 20-fold higher than in nonirradiated counterparts at 24 and 240 hours, respectively (Figure 2A and 2B). Pretreatment with MTT completely blocked the increases in $_{mt}$ROS at both time points. In accordance with the concept that $_{mt}$ROS levels diminish the bioavailability of NO in vascular beds,[39] NO production by HCAECs after irradiation was significantly reduced at both time points, and this effect was abolished by pretreatment with MTT (Figure 2C and 2D).

To dissect the relationship between mitochondrial Ca^{2+} entry and the generation of $_{mt}$ROS, we tested the effects of $_{mt}$ROS scavenging on $\Delta\psi_{mt}$ and Ca^{2+} entry. Irradiation led to an elevation in $\Delta\psi_{mt}$, and this was attenuated by MTT (Figure 3A). As predicted based on $\Delta\psi_{mito}$,

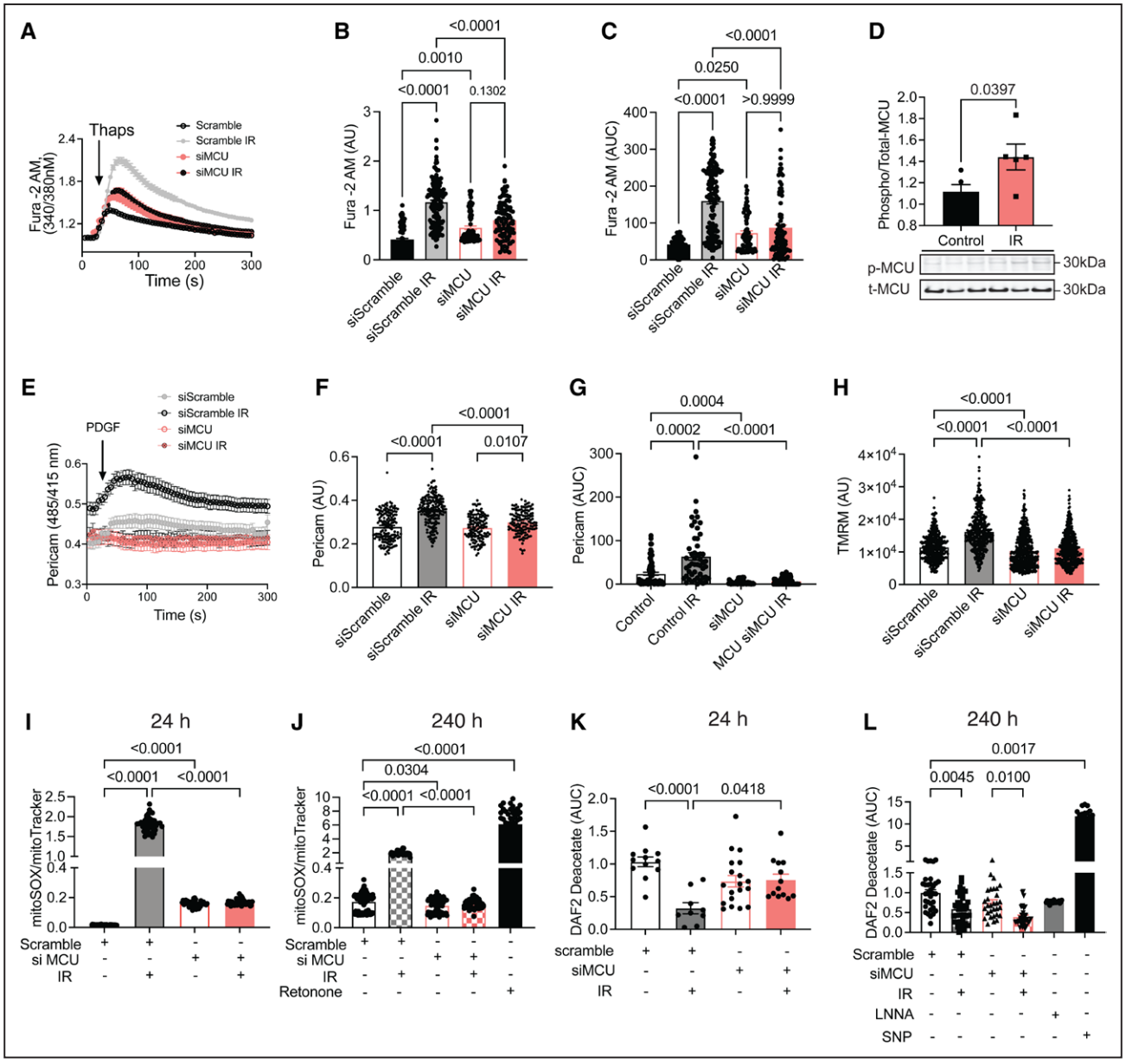

Figure 1. In human umbilical endothelial cells (HUVECs), inhibition of mitochondrial Ca^{2+} entry via MCU (mitochondrial Ca^{2+} uniporter) suppresses irradiation (IR)-induced mitochondrial reactive oxygen species ($_{mt}$ROS) and preserves NO production. All parts compare HUVECs transfected with a scrambled siRNA or siMCU (silencer for MCU RNA) for 72 h IR (4 Gy) to the indicated controls. **A**, Representative Fura-2 AM traces 24 h after IR. **B**, Peak amplitude of Fura-2 AM in response to ATP (100 µM, 1 h) at 24 h after IR, normalized to baseline. **C**, Area under the curve (AUC) for Fura-2 AM recordings in **B**. **D**, Levels of MCU phosphorylation assessed by western blot 24 h following IR. **E**, Representative $_{mt}$Pericam (mitochondrial targeted genetic Ca^{2+} indicator Pericam) traces 24 h after IR. **F**, Baseline of mitochondrial Ca^{2+} levels at 24 h after IR (arbitrary units [AU]). **G**, Area under the curve (AUC) for $_{mt}$Pericam recordings in **E**. **H**, Mitochondrial membrane potential 24 h after IR (4 Gy), as assessed by tetramethylrhodamine methyl ester (TMRM) fluorescence. **I** and **J**, $_{mt}$ROS levels as assessed by mitoSOX fluorescence normalized to mitoTracker fluorescence, at (**I**) 24 and (**J**) 240 h post-IR. **K** and **L**, NO production over 10 min in response to stimulation with PDGF (platelet-derived growth factor), as assessed by DAF2 deacetate (diaminofluorescein diacetate) fluorescence, at (**I**) 24 and (**J**) 240 h after IR. Data are expressed as AUC after subtraction of baseline AUC and are plotted as fold difference relative to untreated cells. Statistical significance was determined by Kruskal-Wallis test. LNNA indicates NG-nitro-L-arginine; p-MCU, phosphorylated MCU; SNP, sodium nitroprusside; and t-MCU, total MCU.

in vehicle-treated cells irradiation increased $[Ca^{2+}]_{mt}$ (Figure 3B) and MTT pretreatment reduced this effect. Moreover, the peak amplitude of the Ca^{2+} transient in response to ATP in irradiated cells was reduced in cells treated with MTT (Figure 3C and 3D). Thus, scavenging of superoxide reduces $\Delta\psi_{mt}$ as well as $[Ca^{2+}]_{mt}$ and Ca^{2+} entry in response to agonists, whereas deletion of MCU reduces $\Delta\psi_{mt}$ and the production of $_{mt}$ROS. These findings imply an inter-relationship of Ca^{2+} entry, the production of $_{mt}$ROS, and $\Delta\psi_{mt}$.

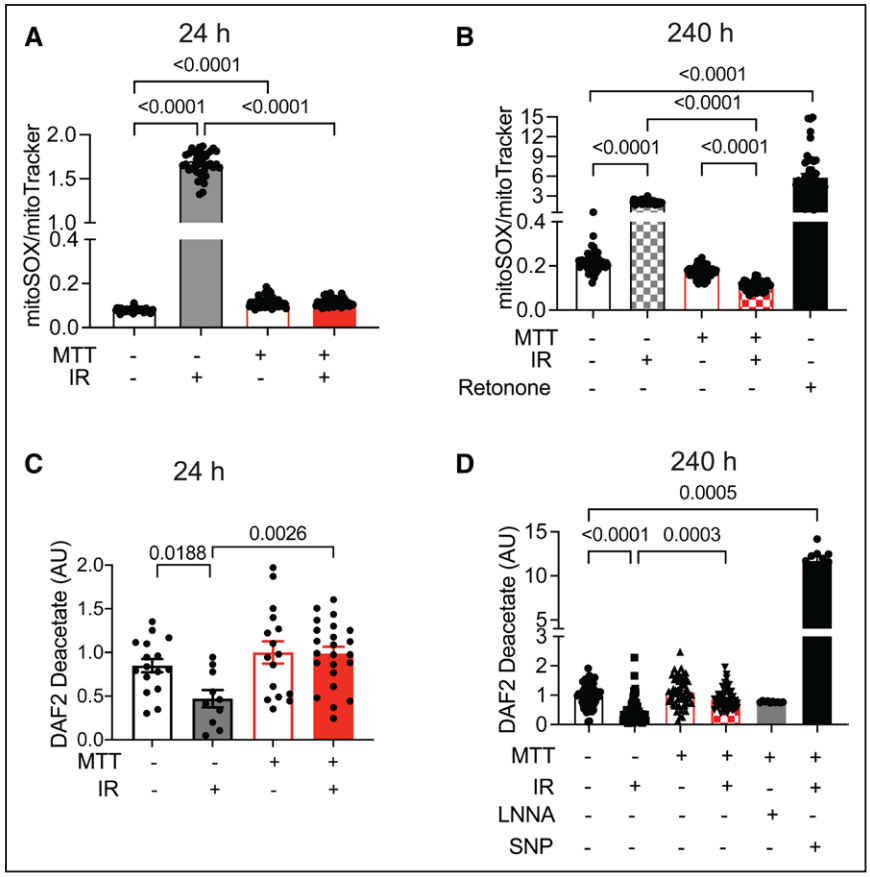

Figure 2. Pretreatment with mitochondrial TEMPO (MTT) prevents irradiation (IR)-induced mitochondrial reactive oxygen species ($_{mt}$ROS) production and loss of NO production in vitro.
A and **B**, MitoSOX fluorescence normalized to mitoTracker fluorescence in human coronary artery endothelial cells (HCAECs) subjected to IR (4 Gy), at (**A**) 24 and (**B**) 240 h after IR, in cells treated with MTT or vehicle starting at 18 h before IR. n=4 independent experiments. **C** and **D**, NO production in response to stimulation with PDGF (platelet-derived growth factor) assessed based on DAF2 deacetate fluorescence (arbitrary units [AU]). NO levels are normalized to baseline (before PDGF addition) and plotted as fold change compared to levels in untreated cells. Images were taken at (**C**) 24 and (**D**) 240 h after IR. Statistical significance was determined by Kruskal-Wallis test. DAF2 diacetate indicates diaminofluorescein diacetate; LNNA, NG-nitro-L-arginine; and SNP, sodium nitroprusside.

Mitochondrial Ca^{2+} Entry Is Required for Irradiation-Induced $_{mt}$ROS Production and Endothelial Dysfunction in Carotid Arteries

We extended the above results from cultured cells to the ex vivo context, examining the extent to which inhibiting mitochondrial Ca^{2+} uptake in the endothelium of carotid arteries protects against irradiation-induced dysfunction. For this purpose, we established and validated a transgenic model in which MCU is selectively deleted in the endothelium (eMCU$^{-/-}$, Figure S2). Endothelium-dependent vasodilation at 24 and 240 hours postirradiation was significantly higher in carotid arteries from irradiation-treated eMCU$^{-/-}$ mice than in those from irradiation-treated wild-type (WT) mice, and similar to that observed in control (no irradiation) WT and eMCU$^{-/-}$ carotid arteries (Figure 4A). To determine whether loss of MCU in the endothelium prevents the reduction of NO after irradiation, we tested the effect of the NO-scavenger, L-NAME, on acetylcholine-induced vasodilation. In WT carotid arteries at 24 hours postirradiation, L-NAME had only a minimal effect (Figure 4B), suggesting that the decrease in vasodilation after irradiation is due to NO deficiency. In carotid arteries of eMCU$^{-/-}$ mice, L-NAME impaired endothelium-dependent relaxation to a similar extent regardless of whether or not they had been irradiated (Figure 4C). At 240 hours after irradiation, endothelial dysfunction was detected in WT but not in eMCU$^{-/-}$ arteries (Figure 4D). Further impairment of endothelium-dependent relaxation in response to L-NAME was seen only in irradiation-treated WT carotid arteries (Figure 4E and 4F), suggesting that the decrease in vasodilation at the later time point is driven in part by factors other than NO deficiency.

Inhibition of Mitochondrial ROS Production Prevents Irradiation-Induced Endothelial Dysfunction and NO Deficiency in Carotid Arteries

To determine whether irradiation-induced production of $_{mt}$ROS leads to endothelial dysfunction, we assessed dilation in response to acetylcholine in the carotid artery of C57BL/6J mice subjected to irradiation (12 Gy X-ray) of the head and neck, in the presence and absence of the mitochondrial ROS scavenger mitoTEMPO (MTT). MTT was administered by continuous infusion using a minipump, starting 3 days before irradiation. At 24 hours postirradiation, relaxation in response to acetylcholine was significantly less pronounced in carotid arteries of irradiation compared to sham-treated mice (Figure 5A). At 48 and 120 hours postirradiation, dilation did not differ significantly between the 2 groups (Figure 5B and 5C), yet at 240 hours postirradiation, a decrease in relaxation in response was observed (Figure 5D). Moreover, infusion

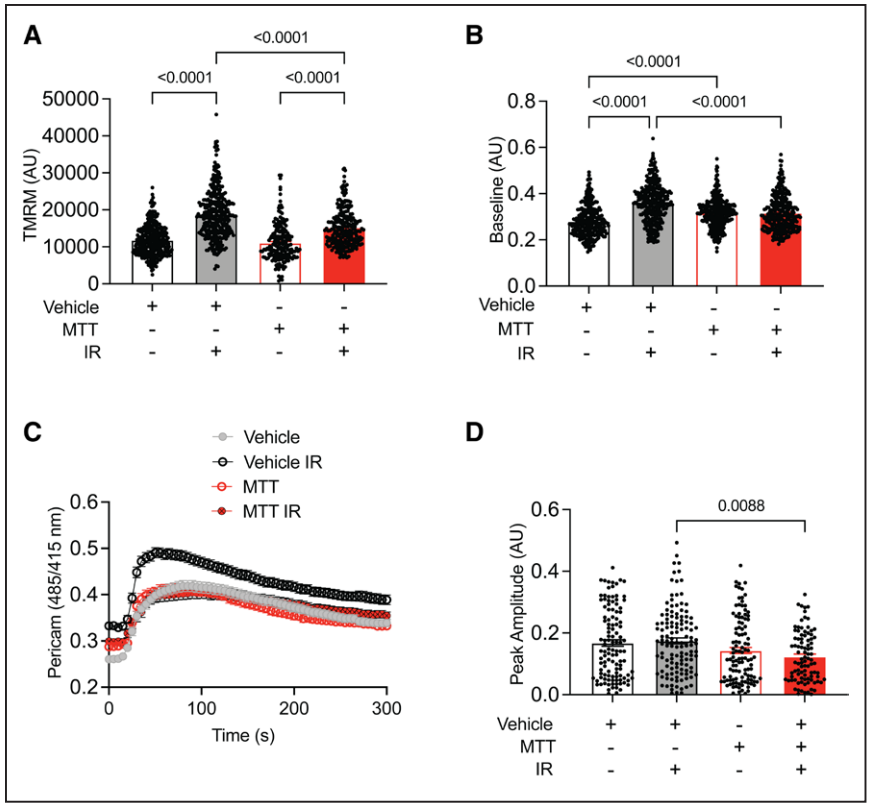

Figure 3. Mitochondrial TEMPO (MTT) prevents irradiation (IR)-induced mitochondrial Ca^{2+} entry and hyperpolarization in vitro. All panels compare human coronary artery endothelial cells (HCAECs) subjected to IR (4 Gy) after pretreatment with mitochondrial TEMPO (MTT; 10 μM). Parameters assessed are (**A**) mitochondrial membrane potential, as determined by tetramethylrhodamine methyl ester (TMRM) fluorescence (arbitrary unit [AU]), at 24 h after IR, (**B**) baseline mitochondrial Ca^{2+} levels, (**C**), mitochondrial Ca^{2+} transients, and (**D**) peak amplitude for $_{mt}$Pericam (mitochondria-targeted genetic Ca^{2+} indicator Pericam) recordings in (**C** and **D**). Statistical significance was determined by Kruskal-Wallis test.

with MTT preserved endothelium-dependent relaxation at 24 and 240 hours postirradiation (Figure 5A through 5D). Notably, endothelium-independent dilation of the carotid artery, that is, relaxation in response to sodium nitroprusside, was similar in all groups (Figure 5E), and this was also the case for endothelium-dependent dilation of mesenteric resistance arteries in response to acetylcholine (Figure 5F). These data indicate that irradiation induces sustained increases in $_{mt}$ROS production locally and that these increases lead to a deficiency in endothelial NO production.

In Cultured Cells and Mice, Mitochondrial DNA Damage Drives Sustained $_{mt}$ROS Production and Reduced NO Production After Irradiation

Next, we sought to identify the mechanism by which irradiation induces $_{mt}$ROS production that persists at 240 hours. We reasoned that excessive ROS is a byproduct of dysregulated activity of the ETC. Because $_{mt}$DNA lacks histones and is located near the ETC, which is the primary source of $_{mt}$ROS, the damage to $_{mt}$DNA from oxidative stress is more extensive and persists longer than that to ($_{nuc}$DNA).[40,41] Sustained $_{mt}$DNA damage could then lead to a further increase in the generation of $_{mt}$ROS by altering the transcription of ETC subunits encoded by $_{mt}$DNA.[40] To test this possibility, we measured the damage to both $_{mt}$DNA and $_{nuc}$DNA in HUVECs after irradiation.

As anticipated, at 24 hours postirradiation, levels of $_{mt}$DNA damage were high, and this persisted at 240 hours (Figure 6A and 6B). In contrast, $_{nuc}$DNA damage was detected only at 24 hours after irradiation (Figure 6C and 6D). Pretreatment of HUVECs with MTT blocked $_{mt}$DNA damage at both timepoints but did not provide protection against $_{nuc}$DNA damage at 24 hours. To confirm that $_{mt}$DNA damage occurs after irradiation in vivo, we also measured $_{mt}$DNA damage in $_{mt}$DNA isolated from the carotid artery of mice after irradiation of the head and neck. A significant increase in damage to $_{mt}$DNA, but not $_{nuc}$DNA, was seen at 24 hours and it persisted at 240 hours postirradiation (comparison was to sham mice). Continuous infusion of MTT prevented $_{mt}$DNA damage after irradiation (Figure 6E and 6F). These data indicate that excess production of mitochondrial superoxide during irradiation induces $_{mt}$DNA damage that is sustained through 240 hours and that it correlates with persistent increases in levels of $_{mt}$ROS and reductions in levels of NO (Figure 2). Having established a feed-forward circuit between Ca^{2+} entry and $_{mt}$ROS (Figures 1 and 3), we also tested DNA damage postirradiation in MCU knockdown HUVECs. This analysis confirmed that $_{mt}$DNA damage was significantly reduced through 240 hours (Figure 6H and 6I) but that $_{nuc}$DNA damage was not (Figure 6J and 6K).

We next tested the effects of acute MCU blockade with Ru265 on irradiation-induced endothelial damage.[22] As expected, pretreatment of HCAECs with Ru265 blocked mitochondrial Ca^{2+} entry (Figure S1D). Like MCU knockdown, this treatment led to decreases in both $_{mt}$ROS levels and $_{mt}$DNA damage (Figure S1E and S1F). This experiment

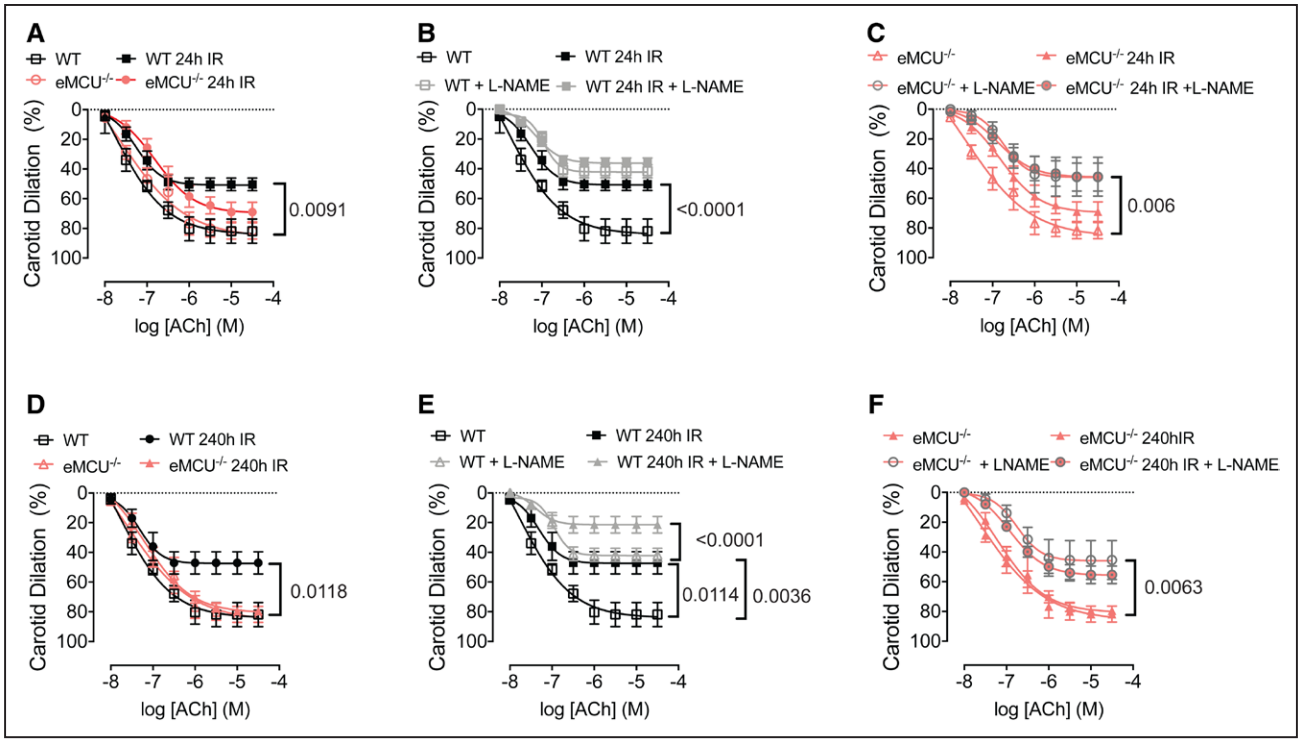

Figure 4. In ex vivo mouse carotid arteries, endothelium-specific deletion of MCU (mitochondrial Ca^{2+} uniporter) protects against endothelial dysfunction following head and neck irradiation (IR).
Dilation of carotid artery in response to cumulative doses of acetylcholine (Ach; endothelium-dependent dilation) in the contexts of the indicated treatments at (**A**–**C**) 24 and (**D**–**F**) 240 h after IR. Effects in (**A** and **D**) wild-type (WT) and eMCU$^{-/-}$ mice, (**B** and **E**) WT type mice pretreated (or not) for 30 min with the eNOS inhibitor N(gamma)-nitro-L-arginine methyl ester (L-NAME), and (**C** and **F**) eMCU$^{-/-}$mice pretreated (or not) with L-NAME for 30 min. n=5 mice per group. *P* values were determined by repeated-measures 2-way ANOVA followed by Tukey post hoc test.

constitutes proof-of-concept evidence that pharmacological inhibition of MCU has the potential to be leveraged to alleviate endothelial injury after irradiation.

To identify a mechanistic link between $_{mt}$DNA damage, changes in levels of $_{mt}$ROS, and changes in the transcription of ETC subunits, we performed quantitative reverse-transcription PCR for the ETC subunits mt-COI and mt-ND1, which are transcribed from $_{mt}$DNA. Exposure to irradiation significantly reduced the transcript levels at 24 and 240 hours (Figure 7A through 7H). Preincubation with Ru265 and MTT prevented this effect (Figure 7A through 7D and Figure 7E through 7H, respectively). In contrast, the transcription of 2 subunits encoded by $_{nuc}$DNA, NDUF1 (NADH dehydrogenase [ubiquinone] 1 alpha subcomplex subunit 1), and COX11 (cytochrome c oxidase 11), was unaffected by irradiation (Figure S3). The dissociation of the transcription of $_{nuc}$DNA- and $_{mt}$DNA-encoded ETC subunits predicts that ETC activity is impaired after irradiation. Indeed, the activity of ETC complex 1 was reduced at 24 hours, and this effect was blocked by inhibiting MCU using Ru265 or by scavenging $_{mt}$ROS with MTT (Figure 7I and 7J). These data delineate a complete pathway by which irradiation leads to increased mitochondrial Ca^{2+} entry via MCU and promotes $_{mt}$ROS production. This causes $_{mt}$DNA damage, which leads to reduced mRNA transcription of ETC subunits and to reduced ETC activity that promotes $_{mt}$ROS production. Increased mitochondrial Ca^{2+} entry and $_{mt}$ROS production correlate with loss of NO.

In Cultured Endothelial Cells, Enhanced Repair of $_{mt}$DNA Protects From Irradiation-Induced Endothelial Injury

To determine whether promoting the repair of $_{mt}$DNA is sufficient to protect against irradiation-induced generation of $_{mt}$ROS and loss of NO, we overexpressed various forms of the enzyme OGG1, which binds to the modified base 8-oxoguanine (produced as a result of oxidative stress) and initiates DNA base-excision repair.[42] Specifically, we expressed a mitochondria-targeted (mito-OGG1), nucleus-targeted OGG1 (nuc-OGG1), and a mitochondria-targeted inactive mutant (R229Q) form (mutt-OGG1). Examination of $_{mt}$DNA in HCAECs revealed that overexpression of mito-OGG1 abolished $_{mt}$DNA injury after irradiation, whereas overexpression of mutt-OGG1 or nuc-OGG1 did not (Figure 8A and 8B). Examination of $_{nuc}$DNA, based on the amplification of β-globin in irradiated versus nonirradiated cells, revealed that overexpression of nuc-OGG1 more effectively restored $_{nuc}$DNA integrity at 24 hours than did mito-OGG1 or mut-OGG1. No significant

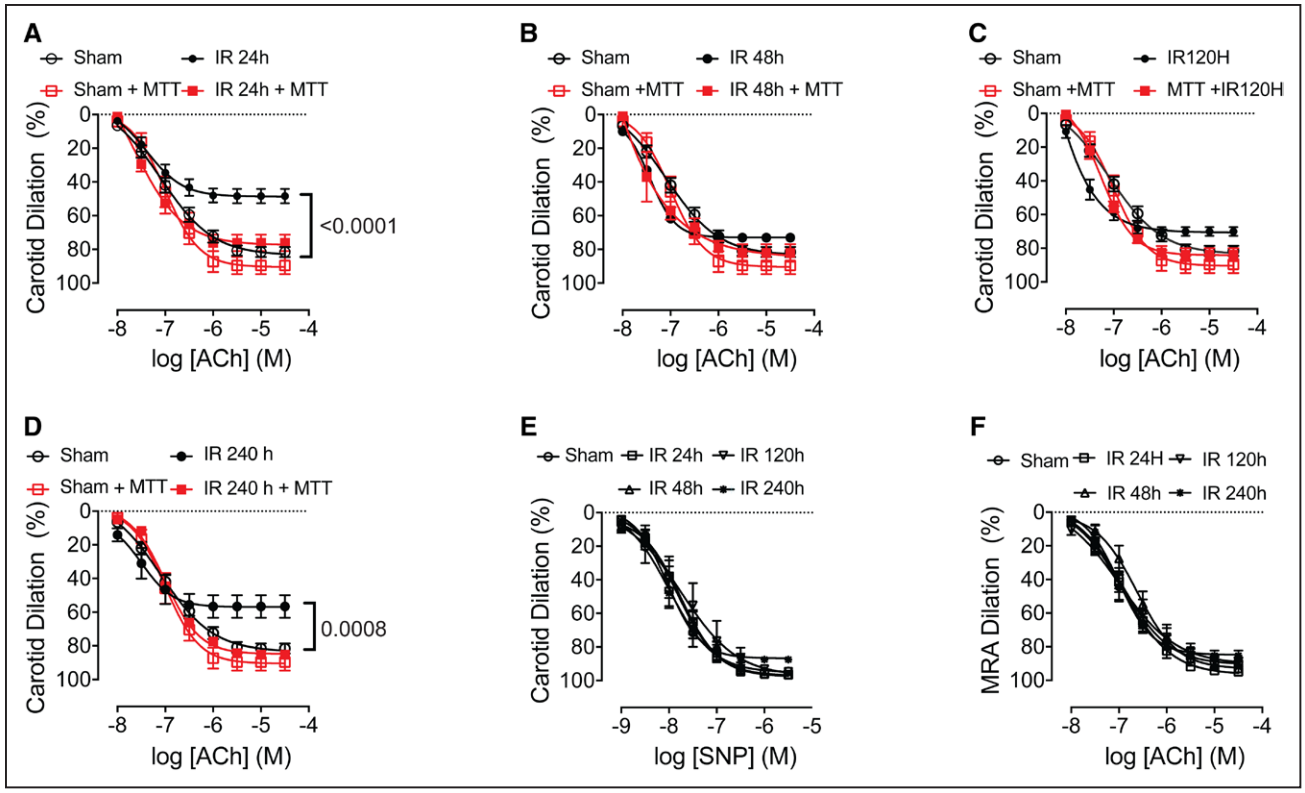

Figure 5. In vivo infusion of mice with mitochondrial TEMPO (MTT) preserves endothelial function following head and neck irradiation (IR).

A–**D**, Acetylcholine (ACh)-induced dilation of the carotid artery in C57BL/6J mice subjected to head and neck irradiation (IR) or sham treatment. Mice were continuously infused with MTT or normal saline starting at 72 h before IR. Dilation was induced at (**A**) 24, (**B**) 48, (**C**) 120, and (**D**) 240 h after IR. **E**, Endothelium-independent dilation of the carotid artery in response to sodium nitroprusside (SNP), in mice subjected to head and neck IR. **F**, Endothelium-dependent dilation of mesenteric resistance arteries (MRAs), in mice subjected to head and neck IR. n=5 mice per group. *P* values were determined by repeat measures 2-way ANOVA followed by Tukey Post hoc test.

irradiation-induced $_{nuc}$DNA damage was present at 240 hours (Figure 8C and 8D).

We then investigated whether $_{mt}$DNA repair blocks irradiation-induced $_{mt}$ROS production. Overexpression of mito-OGG1 in HCAECs eliminated irradiation-induced $_{mt}$ROS production at both 24 and 240 hours postirradiation (Figure 8E and 8F). In contrast, overexpression of nuc-OGG1 or mutt-OGG1 led to significant increases in $_{mt}$ROS production at both 24 and 240 hours after irradiation.

Lastly, we asked whether enhanced $_{mt}$DNA repair after irradiation-induced injury alleviates endothelial dysfunction. Specifically, we tested whether OGG1 overexpression attenuates the deleterious effect of irradiation on endothelial NO bioavailability. HCAECs overexpressing mito-OGG1 were protected from irradiation-induced dysfunction, and levels of NO were similar to those in nonirradiated cells at 240 hours. In contrast, the overexpression of neither mutt-OGG1 nor nuc-OGG1 protected from irradiation-induced loss of NO production (Figure 8G and 8H).

DISCUSSION

Radiation therapy for head and neck cancer is associated with increased risk of atherosclerotic carotid stenosis after a lag period of several years. Here, we report 4 major new findings related to the molecular mechanisms underlying early irradiation-induced carotid endothelial dysfunction and the transition to chronic injury. First, an in vivo block of mitochondrial Ca^{2+} entry via MCU or scavenging of $_{mt}$ROS prevented endothelial dysfunction following irradiation. Second, irradiation promoted mitochondrial Ca^{2+} entry via MCU and production of $_{mt}$ROS. These events were interrelated and led to sustained production of excess $_{mt}$ROS. Third, $_{mt}$DNA damage was identified as a key mechanism driving $_{mt}$ROS production after irradiation. It impaired the transcription of specifically those ETC subunits that are encoded by $_{mt}$DNA as opposed to $_{nuc}$DNA, and it reduced ETC activity. Fourth, these adverse events were prevented by scavenging $_{mt}$ROS or blocking MCU, and either of these 2 manipulations or enhanced repair of $_{mt}$DNA damage prevented the loss of irradiation-induced endothelial NO bioavailability. Collectively, our data delineate a complete pathway by which irradiation disrupts intracellular MCU-mediated Ca^{2+} handling, causes mitochondrial injury, and leads to endothelial dysfunction. We provide strong support for novel approaches to prevent irradiation-induced

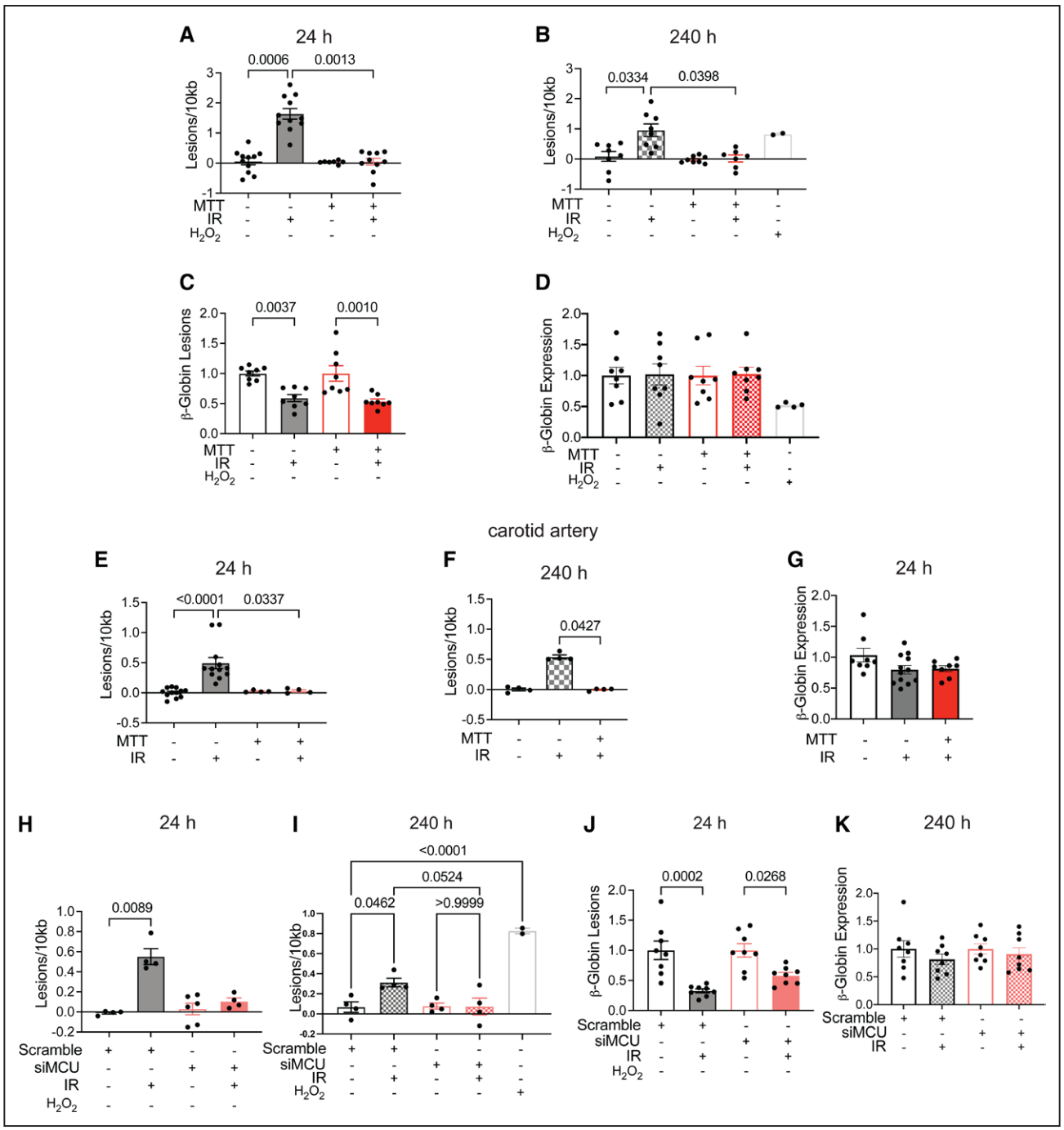

Figure 6. In vitro and in vivo irradiation (IR) induces sustained mitochondrial DNA ($_{mt}$DNA) damage.
A and **B**, Damage to $_{mt}$DNA in human coronary artery endothelial cells, as assessed by polymerase chain reaction (PCR) assay. $_{mt}$DNA lesions at (**A**) 24 and (**B**) 240 h after IR, in cells treated with mitochondrial TEMPO (MTT) or vehicle starting at 18 h before IR. In (**B**), pretreatment with 500 μM H_2O_2 served as a positive control. **C** and **D**, Damage to $_{nuc}$DNA in human umbilical endothelial cells, as assessed by PCR for β-globin. Expression of β-globin at (**C**) 24 and (**D**) 240 h after IR, in cells treated with MTT or vehicle starting at 18 h before IR. In (**D**), pretreatment with 500 μM H_2O_2 served as positive control. **E** and **F**, Damage to $_{mt}$DNA in carotid arteries at (**E**) 24 and (**F**) 240 h after IR. **G**, Copy number of β-globin in the carotid artery at (G) 24 h after IR. **H** and **I**, Lesions in $_{mt}$DNA at (**H**) 24 and (**I**) 240 h post-IR. **J** and **K**, Damage to $_{nuc}$DNA, as assessed by PCR of β-globin from genomic DNA at (**K**) 24 and (**L**) 240 h post-IR. Statistical significance was determined by Kruskal-Wallis test. siMCU indicates silencer for MCU RNA.

vascular dysfunction, based on targeting downstream effectors of excess $_{mt}$ROS and $_{mt}$DNA damage.

These findings are significant because, despite renewed interest in the side effects of cancer therapies on the vascular system, the exact pathogenesis of irradiation-induced arterial wall injury and atherosclerotic disease remains poorly understood. Such injury is of particular clinical relevance for the carotid artery because its

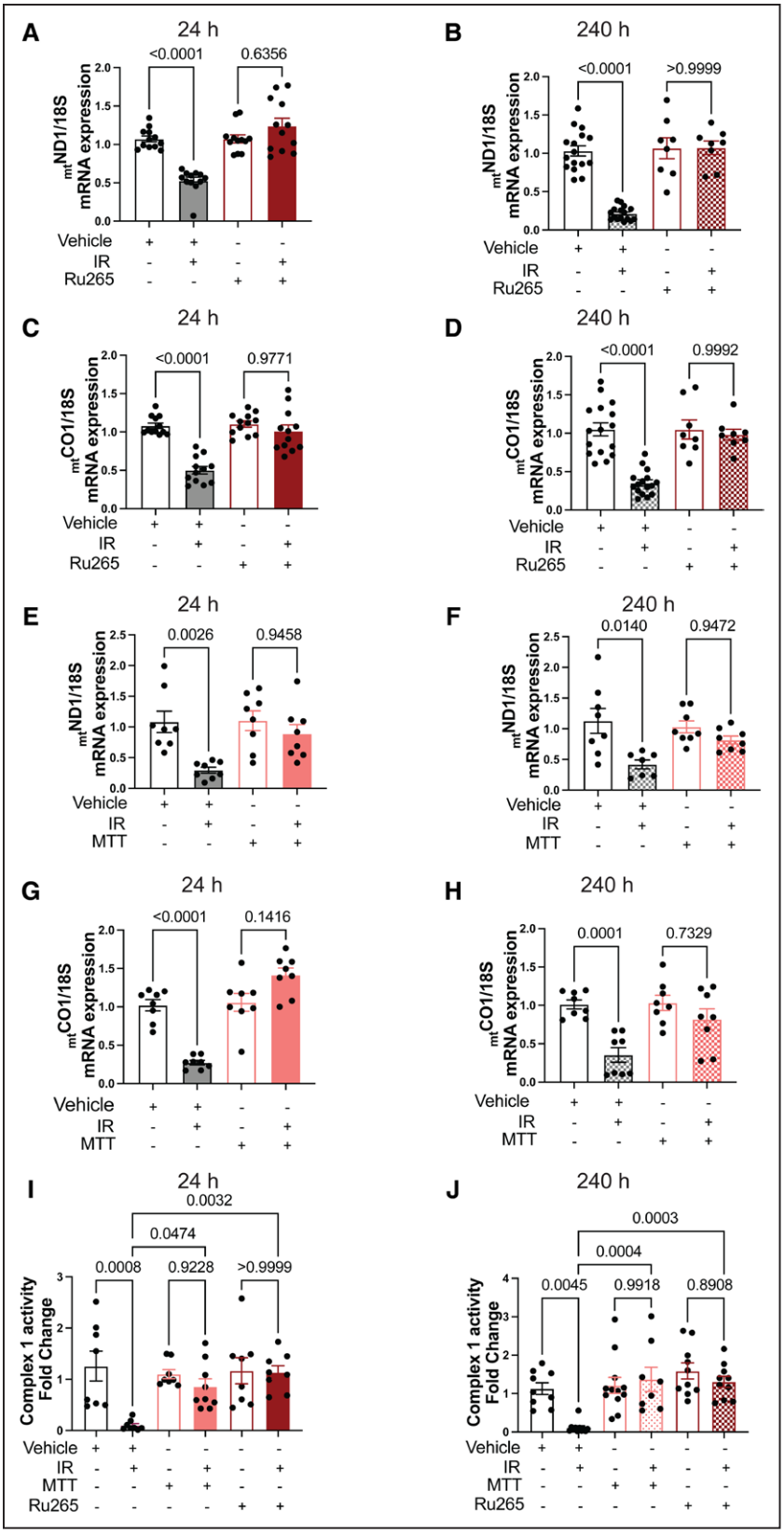

Figure 7. Irradiation (IR)-induced reduction of mitochondrial DNA ($_{mt}$DNA) transcription and ETC (electron transport chain) activity are prevented by mitochondrial reactive oxygen species ($_{mt}$ROS) scavenging or MCU (mitochondrial Ca^{2+} uniporter) inhibition.

A–**D**, Comparison of human coronary artery endothelial cells (HCAECs) pretreated with MCU inhibitor Ru265 (100 μM, 1 h). **A** and **B**, Quantitative reverse-transcription polymerase chain reaction (qRT-PCR) for MT-COI (cytochrome c oxidase I) with cDNA normalized to 100 ng at 24 (**A**) and 240 h (**B**) after IR. **C** and **D,** qRT-PCR for MT-ND1 (NADH-ubiquinone oxidoreductase chain 1) at 24 (**C**) and 240 h (**D**) after IR. **E**–**H**, Comparison of HCAECs pretreated with $_{mt}$ROS scavenger mitochondrial TEMPO (MTT; 10 μM, overnight). **E** and **F**, Quantitative RT-PCR for MT-COI with cDNA normalized to 100ng at 24 (**A**) and 240 h (**B**) after IR. **G** and **H**, qRT-PCR for MT-ND1 at 24 (**C**) and 240 h (**D**) after IR. **I** and **J,** Activity of ETC complex 1 assessed by fluorometric assay at 24 h (**I**) and 240 h (**J**) after IR. Statistical significance was determined by Kruskal-Wallis test.

injury by irradiation is associated with increased risk of cerebrovascular events.[6,8,43,44] The radiation sensitivity of different parts of the vascular wall has been investigated in the past. Irradiation-mediated injury to smooth muscle cells in the medial layer of this vessel has been proposed as the main driver of atherosclerotic disease postirradiation.[45] However, endothelial cells are deemed more sensitive to irradiation than smooth muscle cells.[46,47]

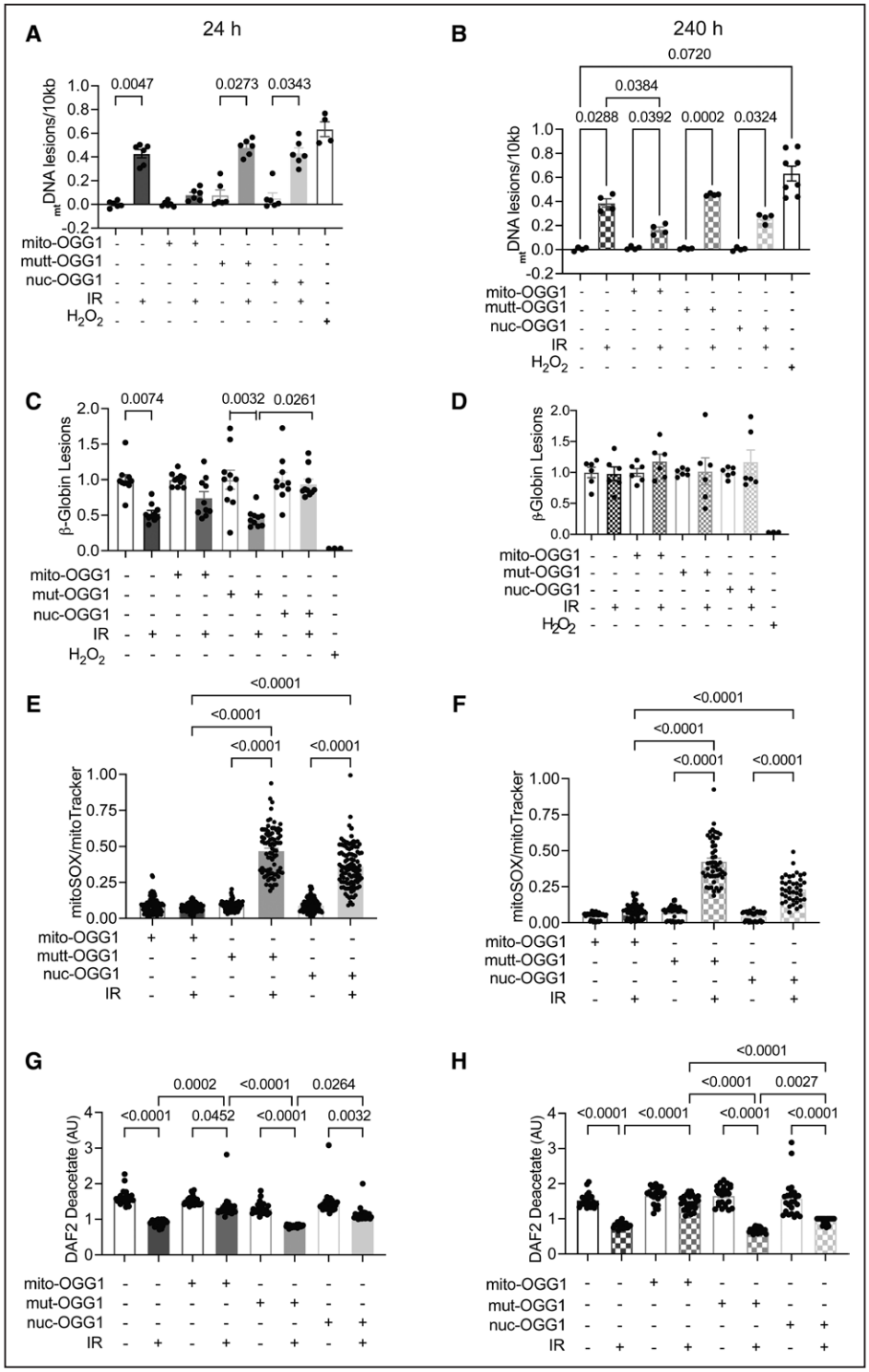

Figure 8. In vitro, enhancement of base-excision repair of mitochondrial DNA ($_{mt}$DNA) protects cells by sustaining mitochondrial reactive oxygen species ($_{mt}$ROS) levels and reducing NO production.

A and **B**, Lesions in $_{mt}$DNA in human coronary artery endothelial cells (HCAECs) transfected with mitochondria-targeted 8-oxoguanine DNA glycosylase (mito-OGG1), mutant mitochondria-targeted OGG1 (mutt-OGG1), or nucleus- targeted OGG1 (nuc-OGG1) for 72 h before irradiation (IR) or sham treatment, as assessed by quantitative reverse-transcription polymerase chain reaction (RT-PCR). Samples were analyzed at (**A**) 24 and (**B**) 240 h post-IR (4 Gy, x-ray). n=4 independent experiments. In both panels, samples pretreated with 500 μM H_2O_2 serve as positive controls. **C** and **D**, Lesions in nuclear DNA ($_{nuc}$DNA) in cells, assessed as in (**A** and **B**), at (**C**) 24 and (**D**) 240 h after IR. In both **C** and **D**, samples pretreated with 500 μM H_2O_2 serve as positive controls. **E** and **F**, MitoSOX fluorescence normalized to mitoTracker fluorescence at (**E**) 24 and (**F**) 240 h after IR. **G** and **H**, NO production in HCAECs at (**G**) 24 and (**H**) 240 h after IR, assessed based on DAF2 deacetate fluorescence (arbitrary units [AU]). NO production was measured after stimulation with PDGF (platelet-derived growth factor). Data were normalized to baseline (before PDGF stimulation) and are plotted as fold difference compared to untreated cells. Statistical significance was determined by Kruskal-Wallis test. DAF2 diacetate indicates diaminofluorescein diacetate.

Numerous studies have reported on molecular pathways that mediate endothelial injury after irradiation in vitro,[46,48] but in vivo evidence that these pathways can be leveraged to reduce irradiation-induced macrovascular disease as provided in this study is scarce.

Irradiation-induced oxidative stress that subsides within seconds of exposure[49] can lead to the initiation of a self-amplifying cycle, giving rise to long-term ROS production[50] and mitochondrial dysfunction. This study reveals that although endothelial cells contain fewer mitochondria than other cell types[51,51] and produce only a small proportion of the energy a cell requires under physiological conditions,[52,53] endothelial damage to $_{mt}$DNA is the key driver of irradiation-induced chronic $_{mt}$ROS production and endothelial dysfunction. These findings are interesting in light of previous observations that excessive $_{mt}$ROS causes sustained inflammatory responses,[54] and NFκB (nuclear factor kappa B) activation in human carotid artery specimens months after irradiation.[12] Given that NFκB is activated by $_{mt}$ROS-driven inflammasomes,[54] we posit that the pathway revealed here lies upstream of sustained NFκB activation after irradiation. Our data are also consistent with seminal work by Yakes and Van Houten,[40] indicating that prolonged exposure to an oxidizing agent results in unrepaired damage to $_{mt}$DNA but not $_{nuc}$DNA. At 24 hours postirradiation, we detected lesions in both $_{mt}$DNA and $_{nuc}$DNA, but at 240 hours, the $_{nuc}$DNA was fully repaired, whereas the $_{mt}$DNA damage persisted. This is further supported by our finding that when base-excision repair was targeted to mitochondria, it fully protected against radiation-induced elevations in $_{mt}$ROS and reduction of NO. Also, our findings that persistent $_{mt}$DNA damage drives long-term increases in $_{mt}$ROS production suggest that pharmacological approaches that activate OGG1 could be leveraged to protect against endothelial impairment following radiation therapy.[55,56]

Previous explanations for the production of $_{mt}$ROS following irradiation were divergent, ranging from increases in the activity of ETC complexes caused by increased ATP demand to reductions in the reentry of protons into the mitochondrial matrix via ETC complex V caused by reversed activity of ATP synthase.[57] In our studies, irradiation led to increased $\Delta\psi_{mt}$, and this effect was abolished by blockade of MCU. We reason that the change in $\Delta\psi_{mt}$ by irradiation is driven by indirect effects of Ca^{2+} in mitochondria, such as increases in metabolic activity, as opposed to a direct effect, given that the entry of positively charged ions would be expected to depolarize the membrane. As a result of the increase in $\Delta\psi_{mt}$, the baseline $[Ca^{2+}]_{mt}$ was elevated in control cells after irradiation. An alternative explanation is that, like other states of high oxidative stress, irradiation promotes posttranscriptional modifications that enhance the Ca^{2+} conductance of the pore-forming subunit of MCU.[58] This is consistent with our discovery that application of the mitochondrial superoxide scavenger MTT reduced $\Delta\psi_{mt}$ and thereby the driving force for entry of Ca^{2+} into the matrix, leading to reductions in the baseline Ca^{2+} concentration and transients (Figure 3). The higher $[Ca^{2+}]_{mt}$ after irradiation may also explain the increase in the mitochondrial transition that was reported in cancer cell lines in the past.[16] Given that MCU inhibition and MTT treatment ultimately reduce mitochondrial levels of superoxide, both preserve integrity of the $_{mt}$DNA and thus endothelial function.

Taken together, we demonstrate that endothelial dilatory dysfunction after irradiation is driven by mitochondrial injury. We also identify an increased mitochondrial membrane potential $\Delta\psi_{mt}$ as the upstream effector of the $_{mt}$ROS production and mitochondrial Ca^{2+} entry that promote each other. Moreover, we establish a feed-forward circuit of $_{mt}$ROS production and $_{mt}$DNA damage that leads to altered ETC activity and a consequent loss of NO bioavailability at early and later time points after irradiation. Our data strongly support the notion that blocking $_{mt}$ROS production and mitochondrial Ca^{2+} uptake using specific inhibitors prevents irradiation-induced vascular dysfunction. These approaches target excess $_{mt}$DNA damage as common downstream effectors.

ARTICLE INFORMATION

Received September 1, 2021; accepted June 20, 2022.

Affiliations

Abboud Cardiovascular Research Center, Department of Internal Medicine (K.A.A., O.M.K., N.R.L., I.M.G.) and Free Radical and Radiation Biology Program, Department of Radiation Oncology (I.M.G.), Carver College of Medicine, University of Iowa. Iowa City VA Healthcare System, Iowa City (I.M.G.).

Acknowledgments

We are grateful for discussions and valuable insights from Dr Muniswamy Madesh for the experiments with Ru265 compound. Dr Joshua J. Woods generously provided the Ru265 compound. We thank Dr Christine Blaumueller of the Scientific Editing and Research Communication Core at the University of Iowa for critical reading of the article and editorial assistance. Experiments in the Radiation and Free Radical Research Core Facility reported in this publication were supported by the National Cancer Institute of the National Institutes of Health under Award Number P30CA086862.

Sources of Funding

This project was supported by grants from the National Institutes of Health (NIH; R01 EY031544 to I.M. Grumbach); the American Heart Association (18IPA 34170003 to I.M. Grumbach); the US Department of Veterans Affairs (I01 BX000163); and the Holden Comprehensive Cancer Center (Institutional Pilot Project Grant, from the American Cancer Society to K. Ait-Aissa).

Disclosures

None.

Supplemental Material

Supplemental Methods
Figures S1–S3
Reference 20

REFERENCES

1. Miller KD, Siegel RL, Lin CC, Mariotto AB, Kramer JL, Rowland JH, Stein KD, Alteri R, Jemal A. Cancer treatment and survivorship statistics, 2016. *CA Cancer J Clin*. 2016;66:271–289. doi: 10.3322/caac.21349
2. Groarke JD, Nguyen PL, Nohria A, Ferrari R, Cheng S, Moslehi J. Cardiovascular complications of radiation therapy for thoracic malignancies: the role

for non-invasive imaging for detection of cardiovascular disease. *Eur Heart J*. 2014;35:612–623. doi: 10.1093/eurheartj/eht114
3. Mertens AC, Yasui Y, Neglia JP, Potter JD, Nesbit ME Jr, Ruccione K, Smithson WA, Robison LL. Late mortality experience in five-year survivors of childhood and adolescent cancer: the childhood cancer survivor study. *J Clin Oncol*. 2001;19:3163–3172. doi: 10.1200/JCO.2001.19.13.3163
4. McCready RA, Hyde GL, Bivins BA, Mattingly SS, Griffen WO Jr. Radiation-induced arterial injuries. *Surgery*. 1983;93:306–312.
5. Sullivan RJ, Flaherty KT. Resistance to BRAF-targeted therapy in melanoma. *Eur J Cancer*. 2013;49:1297–1304. doi: 10.1016/j.ejca.2012.11.019
6. Dorresteijn LD, Kappelle AC, Boogerd W, Klokman WJ, Balm AJ, Keus RB, van Leeuwen FE, Bartelink H. Increased risk of ischemic stroke after radiotherapy on the neck in patients younger than 60 years. *J Clin Oncol*. 2002;20:282–288. doi: 10.1200/JCO.2002.20.1.282
7. Armstrong GT, Oeffinger KC, Chen Y, Kawashima T, Yasui Y, Leisenring W, Stovall M, Chow EJ, Sklar CA, Mulrooney DA, et al. Modifiable risk factors and major cardiac events among adult survivors of childhood cancer. *J Clin Oncol*. 2013;31:3673–3680. doi: 10.1200/JCO.2013.49.3205
8. Murros KE, Toole JF. The effect of radiation on carotid arteries. A review article. *Arch Neurol*. 1989;46:449–455. doi: 10.1001/archneur.1989.00520400109029
9. Sugihara T, Hattori Y, Yamamoto Y, Qi F, Ichikawa R, Sato A, Liu MY, Abe K, Kanno M. Preferential impairment of nitric oxide-mediated endothelium-dependent relaxation in human cervical arteries after irradiation. *Circulation*. 1999;100:635–641. doi: 10.1161/01.cir.100.6.635
10. Zhao W, Robbins ME. Inflammation and chronic oxidative stress in radiation-induced late normal tissue injury: therapeutic implications. *Curr Med Chem*. 2009;16:130–143. doi: 10.2174/092986709787002790
11. Weintraub NL, Jones WK, Manka D. Understanding radiation-induced vascular disease. *J Am Coll Cardiol*. 2010;55:1237–1239. doi: 10.1016/j.jacc.2009.11.053
12. Halle M, Gabrielsen A, Paulsson-Berne G, Gahm C, Agardh HE, Farnebo F, Tornvall P. Sustained inflammation due to nuclear factor-kappa B activation in irradiated human arteries. *J Am Coll Cardiol*. 2010;55:1227–1236. doi: 10.1016/j.jacc.2009.10.047
13. Azzam EI, Jay-Gerin JP, Pain D. Ionizing radiation-induced metabolic oxidative stress and prolonged cell injury. *Cancer Lett*. 2012;327:48–60. doi: 10.1016/j.canlet.2011.12.012
14. Sridharan V, Aykin-Burns N, Tripathi P, Krager KJ, Sharma SK, Moros EG, Corry PM, Nowak G, Hauer-Jensen M, Boerma M. Radiation-induced alterations in mitochondria of the rat heart. *Radiat Res*. 2014;181:324–334. doi: 10.1667/RR13452.1
15. Kim GJ, Fiskum GM, Morgan WF. A role for mitochondrial dysfunction in perpetuating radiation-induced genomic instability. *Cancer Res*. 2006;66:10377–10383. doi: 10.1158/0008-5472.CAN-05-3036
16. Leach JK, Van Tuyle G, Lin PS, Schmidt-Ullrich R, Mikkelsen RB. Ionizing radiation-induced, mitochondria-dependent generation of reactive oxygen/nitrogen. *Cancer Res*. 2001;61:3894–3901.
17. Roy SJ, Koval OM, Sebag SC, Ait-Aissa K, Allen BG, Spitz DR, Grumbach IM. Inhibition of CaMKII in mitochondria preserves endothelial barrier function after irradiation. *Free Radic Biol Med*. 2020;146:287–298. doi: 10.1016/j.freeradbiomed.2019.11.012
18. Spitz DR, Sim JE, Ridnour LA, Galoforo SS, Lee YJ. Glucose deprivation-induced oxidative stress in human tumor cells. A fundamental defect in metabolism? *Ann N Y Acad Sci*. 2000;899:349–362. doi: 10.1111/j.1749-6632.2000.tb06199.x
19. Aykin-Burns N, Ahmad IM, Zhu Y, Oberley LW, Spitz DR. Increased levels of superoxide and H2O2 mediate the differential susceptibility of cancer cells versus normal cells to glucose deprivation. *Biochem J*. 2009;418:29–37. doi: 10.1042/BJ20081258
20. Denton RM. Regulation of mitochondrial dehydrogenases by calcium ions. *Biochim Biophys Acta*. 2009;1787:1309–1316. doi: 10.1016/j.bbabio.2009.01.005
21. Chatterjee A, Mambo E, Zhang Y, Deweese T, Sidransky D. Targeting of mutant hogg1 in mammalian mitochondria and nucleus: effect on cellular survival upon oxidative stress. *BMC Cancer*. 2006;6:235. doi: 10.1186/1471-2407-6-235
22. Woods JJ, Nemani N, Shanmughapriya S, Kumar A, Zhang M, Nathan SR, Thomas M, Carvalho E, Ramachandran K, Srikantan S, et al. A selective and cell-permeable Mitochondrial Calcium Uniporter (MCU) inhibitor preserves mitochondrial bioenergetics after hypoxia/reoxygenation injury. *ACS Cent Sci*. 2019;5:153–166. doi: 10.1021/acscentsci.8b00773
23. Kwong JQ, Lu X, Correll RN, Schwanekamp JA, Vagnozzi RJ, Sargent MA, York AJ, Zhang J, Bers DM, Molkentin JD. The mitochondrial calcium uniporter selectively matches metabolic output to acute contractile stress in the Heart. *Cell Rep*. 2015;12:15–22. doi: 10.1016/j.celrep.2015.06.002
24. Forde A, Constien R, Gröne HJ, Hämmerling G, Arnold B. Temporal Cre-mediated recombination exclusively in endothelial cells using Tie2 regulatory elements. *Genesis*. 2002;33:191–197. doi: 10.1002/gene.10117
25. Madisen L, Zwingman TA, Sunkin SM, Oh SW, Zariwala HA, Gu H, Ng LL, Palmiter RD, Hawrylycz MJ, Jones AR, et al. A robust and high-throughput Cre reporting and characterization system for the whole mouse brain. *Nat Neurosci*. 2010;13:133–140. doi: 10.1038/nn.2467
26. Wong J, Armour E, Kazanzides P, Iordachita I, Tryggestad E, Deng H, Matinfar M, Kennedy C, Liu Z, Chan T, et al. High-resolution, small animal radiation research platform with x-ray tomographic guidance capabilities. *Int J Radiat Oncol Biol Phys*. 2008;71:1591–1599. doi: 10.1016/j.ijrobp.2008.04.025
27. Wang YF, Lin SC, Na YH, Black PJ, Wuu CS. Dosimetric verification and commissioning for a small animal image-guided irradiator. *Phys Med Biol*. 2018;63:145001. doi: 10.1088/1361-6560/aacdcd
28. Dikalova AE, Bikineyeva AT, Budzyn K, Nazarewicz RR, McCann L, Lewis W, Harrison DG, Dikalov SI. Therapeutic targeting of mitochondrial superoxide in hypertension. *Circ Res*. 2010;107:106–116. doi: 10.1161/CIRCRESAHA.109.214601
29. Nagai T, Sawano A, Park ES, Miyawaki A. Circularly permuted green fluorescent proteins engineered to sense Ca^{2+}. *Proc Natl Acad Sci U S A*. 2001;98:3197–3202. doi: 10.1073/pnas.051636098
30. Mols M, Ceragioli M, Abee T. Heat stress leads to superoxide formation in Bacillus cereus detected using the fluorescent probe MitoSOX. *Int J Food Microbiol*. 2011;151:119–122. doi: 10.1016/j.ijfoodmicro.2011.08.004
31. Raut GK, Chakrabarti M, Pamarthy D, Bhadra MP. Glucose starvation-induced oxidative stress causes mitochondrial dysfunction and apoptosis via Prohibitin 1 upregulation in human breast cancer cells. *Free Radic Biol Med*. 2019;145:428–441. doi: 10.1016/j.freeradbiomed.2019.09.020
32. Berkels R, Dachs C, Roesen R, Klaus W. Simultaneous measurement of intracellular $Ca^{(2+)}$ and nitric oxide: a new method. *Cell Calcium*. 2000;27:281–286. doi: 10.1054/ceca.2000.0119
33. Santos JH, Meyer JN, Mandavilli BS, Van Houten B. *Quantitative PCR-based measurement of nuclear and mitochondrial DNA damage and repair in mammalian cells DNA repair protocols*. Springer; 2006: 183–199.
34. Van Houten B, Chandrasekhar D, Huang W, Katz E. Mapping DNA lesions at the gene level using quantitative PCR methodology. *Amplifications*. 1993;10:10–17.
35. Lee Y, Park J, Lee G, Yoon S, Min CK, Kim TG, Yamamoto T, Kim DH, Lee KW, Eom SH. S92 phosphorylation induces structural changes in the N-terminus domain of human mitochondrial calcium uniporter. *Sci Rep*. 2020;10:9131. doi: 10.1038/s41598-020-65994-y
36. Joiner ML, Koval OM, Li J, He BJ, Allamargot C, Gao Z, Luczak ED, Hall DD, Fink BD, Chen B, et al. CaMKII determines mitochondrial stress responses in heart. *Nature*. 2012;491:269–273. doi: 10.1038/nature11444
37. Landmesser U, Dikalov S, Price SR, McCann L, Fukai T, Holland SM, Mitch WE, Harrison DG. Oxidation of tetrahydrobiopterin leads to uncoupling of endothelial cell nitric oxide synthase in hypertension. *J Clin Invest*. 2003;111:1201–1209. doi: 10.1172/JCI14172
38. Förstermann U, Münzel T. Endothelial nitric oxide synthase in vascular disease: from marvel to menace. *Circulation*. 2006;113:1708–1714. doi: 10.1161/CIRCULATIONAHA.105.602532
39. Widlansky ME, Gutterman DD. Regulation of endothelial function by mitochondrial reactive oxygen species. *Antioxid Redox Signal*. 2011;15:1517–1530. doi: 10.1089/ars.2010.3642
40. Yakes FM, Van Houten B. Mitochondrial DNA damage is more extensive and persists longer than nuclear DNA damage in human cells following oxidative stress. *Proc Natl Acad Sci U S A*. 1997;94:514–519. doi: 10.1073/pnas.94.2.514
41. Richter C, Park JW, Ames BN. Normal oxidative damage to mitochondrial and nuclear DNA is extensive. *Proc Natl Acad Sci U S A*. 1988;85:6465–6467. doi: 10.1073/pnas.85.17.6465
42. Ba X, Boldogh I. 8-Oxoguanine DNA glycosylase 1: Beyond repair of the oxidatively modified base lesions. *Redox Biol*. 2018;14:669–678. doi: 10.1016/j.redox.2017.11.008
43. Venkatesulu BP, Mahadevan LS, Aliru ML, Yang X, Bodd MH, Singh PK, Yusuf SW, Abe J-I, Krishnan S. Radiation-induced endothelial vascular injury: a review of possible mechanisms. *JACC Basic Transl Sci*. 2018;3:563–572. doi: 10.1016/j.jacbts.2018.01.014
44. Fonkalsrud EW, Sanchez M, Zerubavel R, Mahoney A. Serial changes in arterial structure following radiation therapy. *Surg Gynecol Obstet*. 1977;145:395–400.

45. Donis N, Oury C, Moonen M, Lancellotti P. Treating cardiovascular complications of radiotherapy: a role for new pharmacotherapies. *Expert Opin Pharmacother*. 2018;19:431–442. doi: 10.1080/14656566.2018.1446080
46. Baselet B, Sonveaux P, Baatout S, Aerts A. Pathological effects of ionizing radiation: endothelial activation and dysfunction. *Cell Mol Life Sci*. 2019;76:699–728. doi: 10.1007/s00018-018-2956-z
47. Dimitrievich GS, Fischer-Dzoga K, Griem ML. Dimetrievich. Radiosensitivity of vascular tissue I differential radiosensitivity of capillaries- a quantitative in vivo study. *Radiat Res*. 1984;99:511–535.
48. Roy SJ, Koval OM, Sebag SC, Ait-Aissa K, Allen BG, Spitz DR, Grumbach IM. Inhibition of CaMKII in mitochondria preserves endothelial barrier function after irradiation. *Free Radic Biol Med*. 2020;146:287–298. doi: 10.1016/j.freeradbiomed.2019.11.012
49. Riley PA. Free radicals in biology: oxidative stress and the effects of ionizing radiation. *Int J Radiat Biol*. 1994;65:27–33. doi: 10.1080/09553009414550041
50. Yamamori T, Yasui H, Yamazumi M, Wada Y, Nakamura Y, Nakamura H, Inanami O. Ionizing radiation induces mitochondrial reactive oxygen species production accompanied by upregulation of mitochondrial electron transport chain function and mitochondrial content under control of the cell cycle checkpoint. *Free Radic Biol Med*. 2012;53:260–270. doi: 10.1016/j.freeradbiomed.2012.04.033
51. Kluge MA, Fetterman JL, Vita JA. Mitochondria and endothelial function. *Circ Res*. 2013;112:1171–1188. doi: 10.1161/CIRCRESAHA.111.300233
52. Ibrahim A, Yucel N, Kim B, Arany Z. Local Mitochondrial ATP Production Regulates Endothelial Fatty Acid Uptake and Transport. *Cell Metab*. 2020;32:309–319.e7. doi: 10.1016/j.cmet.2020.05.018
53. Culic O, Gruwel ML, Schrader J. Energy turnover of vascular endothelial cells. *Am J Physiol*. 1997;273(1 Pt 1):C205–C213. doi: 10.1152/ajpcell.1997.273.1.C205
54. Sebag SC, Koval OM, Paschke JD, Winters CJ, Jaffer OA, Dworski R, Sutterwala FS, Anderson ME, Grumbach IM. Mitochondrial CaMKII inhibition in airway epithelium protects against allergic asthma. *JCI Insight*. 2017;2:e88297. doi: 10.1172/jci.insight.88297
55. Baptiste BA, Katchur SR, Fivenson EM, Croteau DL, Rumsey WL, Bohr VA. Enhanced mitochondrial DNA repair of the common disease-associated variant, Ser326Cys, of hOGG1 through small molecule intervention. *Free Radic Biol Med*. 2018;124:149–162. doi: 10.1016/j.freeradbiomed.2018.05.094
56. Kiyooka T, Ohanyan V, Yin L, Pung YF, Chen YR, Chen CL, Kang PT, Hardwick JP, Yun J, Janota D, et al. Mitochondrial DNA integrity and function are critical for endothelium-dependent vasodilation in rats with metabolic syndrome. *Basic Res Cardiol*. 2022;117:3. doi: 10.1007/s00395-021-00908-1
57. Rai Y, Pathak R, Kumari N, Sah DK, Pandey S, Kalra N, Soni R, Dwarakanath BS, Bhatt AN. Mitochondrial biogenesis and metabolic hyperactivation limits the application of MTT assay in the estimation of radiation induced growth inhibition. *Sci Rep*. 2018;8:1531. doi: 10.1038/s41598-018-19930-w
58. Dong Z, Shanmughapriya S, Tomar D, Siddiqui N, Lynch S, Nemani N, Breves SL, Zhang X, Tripathi A, Palaniappan P, et al. Mitochondrial Ca^{2+} uniporter is a mitochondrial luminal redox sensor that augments MCU channel activity. *Mol Cell*. 2017;65:1014–1028.e7. doi: 10.1016/j.molcel.2017.01.032